Supplemental material for
Probing the in-situ Elastic Nonlinearity of Rocks With Earth Tides and Seismic Noise

Christoph Sens-Schönfelder*
Helmholtz Centre Potsdam - GFZ German Research Centre for Geosciences, Germany

Tom Eulenfeld
Institute of Geosciences, Friedrich Schiller University Jena, Germany
(Dated: April 5, 2019)

I. CALCULATION OF NOISE CORRELATION FUNCTIONS

We calculate ambient noise correlation functions (NCF) for all 6 pairs of the north-south, east-west and up-down components of the seismic station PATCX using the ObsPy software package [1]. The noise is processed starting from 24 h long records on which we perform the following pre-processing steps

1. decimation to 50 Hz,
2. bandpass filtering between 3 Hz and 7 Hz,
3. muting of seismic events with amplitudes above ten time the median of the absolute amplitude.

After this, the 24 h records are subdivided into 10 min long sequences that are detrended and 1-bit normalized before being correlated. The NCFs are filtered between 4 and 6 Hz. We denote the correlation functions $\phi_{X,Y}(t,\tau)$ indicating the correlation of component X with component Y for $X,Y \in (Z,N,E)$ of the 10 min long noise sequence centred around time t with correlation time lag τ. Time t is discretized in increments of 10 min and while the discretization of τ is given by the sampling rate. For the time span of 11 years we obtain roughly 580.000 correlation functions for each of the six component pairs.

II. MEASUREMENT OF VELOCITY CHANGES WITH STRETCHING

To infer the seismic velocity changes in the subsurface that best explains the changes observed in the noise correlation functions we apply the stretching method [2, 3] that simulates a spatially homogeneous change of the propagation velocity. Measurements of the velocity *change* are relative measurements performed against a stretched reference $\psi_{X,Y}(\xi,\tau)$, where τ indicates lapse time again and ξ indicates the parameter of the stretching transformation Σ defined as:

$$\Sigma : (\psi_{X,Y}(\tau),\xi) : \psi_{X,Y}(\tau) \mapsto \psi_{X,Y}(\exp(\xi)\tau)\,. \qquad (1)$$

We use $\psi_{X,Y}(e^{\xi}\tau) = \psi_{X,Y}(\xi,\tau)$. Comparison between the noise correlation functions $\phi_{X,Y}(t,\tau)$ and the stretched references $\psi_{X,Y}(\xi,\tau)$ is done by means of the correlation coefficient in a certain lapse time window between start-time τ_s and end-time τ_e:

$$C^{\tau_s,\tau_e}_{X,Y}(t,\xi) = \frac{\int_{\tau_s}^{\tau_e} \psi_{X,Y}(\xi,\tau')\phi_{X,Y}(t,\tau')d\tau'}{\sqrt{\int_{\tau_s}^{\tau_e} \psi_{X,Y}(\xi,\tau')^2 d\tau' \int_{\tau_s}^{\tau_e} \phi_{X,Y}(t,\tau')^2 d\tau'}}. \qquad (2)$$

We call $C^{\tau_s,\tau_e}_{X,Y}(t,\xi)$ the similarity matrix that quantifies the match between a NCF and a reference trace that can be obtained with different amounts of stretching. The most likely velocity change is obtained by selecting the stretching with the highest value of C

$$\Xi^{\tau_s,\tau_e}_{X,Y}(t) = arg\ \max_{\xi} C^{\tau_s,\tau_e}_{X,Y}(t,\xi) \qquad (3)$$

To stabilize the measurements we make use of (A) the measurements obtained from different combinations of components that reflect the same material change and (B) the temporal oversampling at a rate of 10 min that can potentially be reduced. To utilize this redundancy we could average $\Xi^{\tau_s,\tau_e}_{X,Y}(t)$ for all combinations of X and Y or apply a smoothing over the time axis. This approach would linearly down-weight outliers that could be caused by poor convergence of the NCF or by cycle skipping [4]. Here we suggest to perform the averaging and smoothing operations at the level of the similarity matrices $C^{\tau_s,\tau_e}_{X,Y}(t,\xi)$ which can further suppress the influence of outliers [5]. The final observation of the best fitting stretching is

$$\Xi^{\tau_s,\tau_e}(t) = arg\ \max_{\xi} \bar{C}^{\tau_s,\tau_e}(t,\xi) \qquad (4)$$

where $\bar{C} = 1/6 \sum_P C_P$ with $P \in (ZZ, ZN, ZE, NN, NE, EE)$. In the same way a temporal smoothing is done by smoothing the similarity matrices along the time axis before the best fitting stretching is estimated from the location of the maxima along the ξ-axis. The relative velocity change is finally

$$\frac{dv}{v}^{\tau_s,\tau_e}(t) = \Xi^{\tau_s,\tau_e}(t) \qquad (5)$$

To avoid degradation of the reference trace when traces are stacked that are significantly stretched ($1/f <$

* sens-schoenfelder@gfz-potsdam.de

$0.25\tau \times \mathrm{d}v/v$ for frequency f and lapse time τ) due to the variable subsurface velocities we construct the references iteratively [4, 6]. We estimate a preliminary reference trace by stacking all available correlation functions of the 11 years and use it to estimate a preliminary velocity change. The effect of this velocity change is corrected for by appropriate stretching before a final reference trace is constructed by averaging the corrected correlation functions. Since the 10 min sampling leads to a large number of correlations functions, this procedure is applied on chunks of 20 days length. This has the advantage that the reference is automatically adapted to slow changes in the material that lead to decreasing similarity between NCFs with increasing temporal separation[5, 7]. Using a new reference every 20 days accounts for this. To construct a continuous observation time series for the whole period the similarity matrices for the 20 day chunks are corrected for their relative offset, and concatenated. The relative offset between the similarity matrices originates in the velocity change between the references of the different chunks and is measured with the stretching method exactly as the velocity change is measured within the chunks.

III. ERROR ESTIMATION OF SENSITIVITY MEASUREMENTS

We obtain a velocity-strain sensitivity $\left|\frac{\mathrm{d}v/v}{\epsilon_\mathrm{V}}\right| = 8 \pm 2 \times 10^3$ with a phase lag of 150 ± 15 min for the M_2 constituent. The error bounds are estimated here by splitting the 11 years long time series into 22 segments of 1 year duration with 50 % overlap. The standard deviation of the phase difference (15 min) is used as its error. We use the logarithmic mean and its standard deviation to obtain the mean sensitivity (8×10^3) and its confidence interval ($6.5e \times 10^3$) from the measurements in the different segments.

IV. PHASE RELATION BETWEEN SEISMIC VELOCITY, TEMPERATURE AND TIDAL STRAIN

We illustrate the distinctive influences of temperature and strain in Figure S1 where we show periodic stacks with the fundamental frequencies of lunar and solar processes. Figure S1a and b show stacks of the velocity signal with periodicity of 1 d^{-1} (S_1) and 1.932 d^{-1} (M_2), respectively. In both cases a nearly sinusoidal oscillation of the velocity at the stacking frequency is observed. Figures S1c and d show similar stacks of the air temperature measured at creepmeter installation CHO2 32 km south of station PATCX and the volumetric tidal strain calculated for the location of PATCX. At a stacking frequency of 1 d^{-1} (Fig. S1c) the average daily temperature curve shows a slightly skewed sine while the strain does not show any oscillation with a 1 d period. Instead the volumetric strain varies with two oscillations per day corresponding to the principal solar semidiurnal tide S_2. Comparing Figures S1a and c the seismic velocity changes are well correlated with the daily temperature variations as shown earlier[4]. The velocity shows a slight time delay of 1 h compared to the temperature[4]. This velocity signal is not related to the tidal constituent S_1 of the sun but rather to the sun's radiation effect. The non-sinusoidal shape of the temperature variation and velocity signal causes overtones at multiples of the 1 d^{-1} fundamental frequency.

We attribute the excess amplitude of the velocity signal at 2 d^{-1} (S_2) and the peaks around 4 d^{-1} (θ_4) to overtones of the radiation effect. The sidebands of the 1 d^{-1}, 2 d^{-1} and 4 d^{-1} peaks (P_1, K_1, T_2, R_2, θ_{4+}, θ_{4-}) in Figure 2 of the main text likely reflect an annual modulation of the radiation effect. K_1 additionally has a significant contribution from tidal strain.

The periodic stack of temperature and strain at 1.932 d^{-1} (Figure S1d) averages out all temperature fluctuations but coherently adds up the strain signal of the principal lunar semidiurnal tide M_2. Since compressional strain is negative, there is an inverse relation between velocity and strain with a time lag of 2.5 h. This supports the volumetric tidal strain as the most likely cause of the velocity variation at the M_2 period.

V. NONLINEAR INTERACTION OF VELOCITY VARIATIONS WITH TIDAL AND THERMAL ORIGIN

As a simple model for the modulation process we assume that the observed signal $s(t)$ — the measured velocity variation — consists of the individual constituents $s_1(t)$ and $s_2(t)$ that we approximate with $s_i(t) = A_i \cos(2\pi f_i t + \phi_i)$ plus their product $A_1 A_2 \cos(2\pi f_1 t + \phi_1) \cos(2\pi f_2 t + \phi_2)$ scaled by a constant C. The modulation signal can be represented by two oscillations of amplitude $0.5CA_1A2$ at the sum and the difference of the original frequencies $f_1 \pm f_2$:

$$\begin{aligned} s(t) = A_1 \cos(2\pi f_1 t + \phi_1) + A_2 \cos(2\pi f_2 t + \phi_2) \quad (6) \\ + \frac{1}{2} C A_1 A_2 \cos(2\pi t(f_1 + f_2) + \phi_1 + \phi_2) \\ + \frac{1}{2} C A_1 A_2 \cos(2\pi t(f_1 - f_2) + \phi_1 - \phi_2) \end{aligned}$$

Since $s_1(t)$, $s_2(t)$ and the two interaction terms are separated in frequency, we can retrieve the average signals by cyclic averaging as in Figure S1. We expect the strongest modulation signal to be generated by the interaction between the strain signal from the M_2 tide ($f_1 = 1.932$ d^{-1}) and the thermal signal with a daily cycle S_1 ($f_2 = 1$ d^{-1}).

We use the following approach to verify that the hypothesis of cross-modulation is compatible with the observations beyond the sheer presence of spectral peaks. The modulation signals which can directly be retrieved from the data by cyclic averaging at $f_1 \pm f_2$ are shown

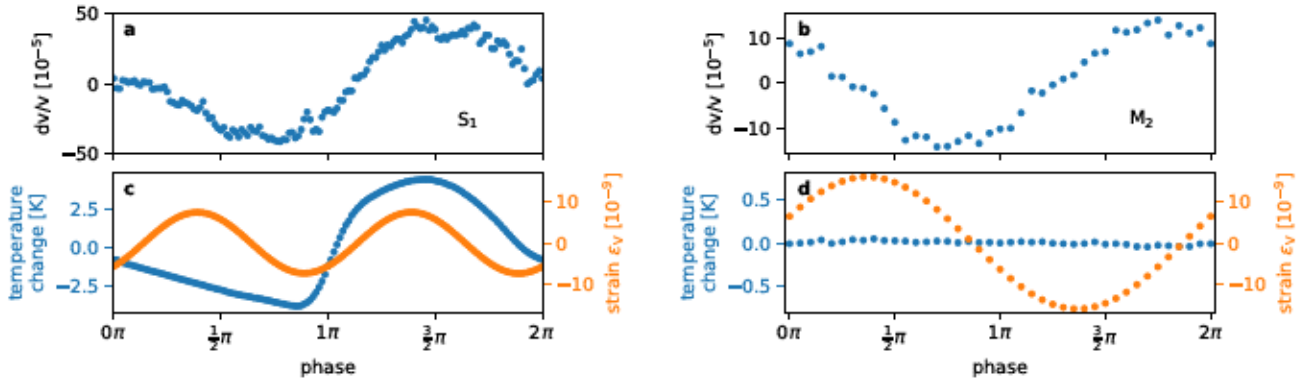

FIG. S1. Comparison between seismic velocity changes, air temperature and tidal strain for different periodicities. **a**) and **b**) show the cyclic averages of the velocity variations with stacking periods of 24 h (S_1) and 12.42 h (M_2), respectively. **c**) and **d**) show the corresponding stacks of air temperature and tidal strain. Uncertainties can be judged from the short term fluctuations.

in Figure S2 with continuous lines. With amplitudes of $\frac{dv}{v} \approx 0.0025$ % these signals are very small but robustly reconstructed due to the long time series. To generate the synthetic modulation signals we use the periodically averaged curves of the M_2 and S_1 velocity signals with the frequencies f_1 and f_2 shown in Figure S1. These signals are periodically replicated to form clean time series $\tilde{s}_1$ and $\tilde{s}_2$ of the two generating signals with the same duration as the original observation. The synthetic modulation signals are then obtained as the cyclic averages of $C\tilde{s}_1(t)\tilde{s}_2(t)$ at the two frequencies $f_1 + f_2 = 2.932$ d^{-1} and $f_1 - f_2 = 0.932$ d^{-1}. The dashed lines Figure S2 show the synthetic modulation signals at the two frequencies for a constant $C = -1000$. Both signals can be explained reasonably well in amplitude and phase with a single constant C. The negative sign of C indicates that the signals suppress each other leading to a smaller amplitude of the modulated signals compared to the linear superposition.

We do neither see evidence for a nonlinearity in the velocity response to strain of different tidal constituents (Figure 4 of the main text), nor do we observe any sign of self-modulation of the M_2 tidal signal that would cause a spectral peak at twice the M_2 frequency. This means that the physical character of the tidal and radiation perturbation mechanisms must be different. We speculate that the difference between the effects of tidal strain and thermal strain is due to the spatial shape and orientation of the two strain fields.

VI. AMBIENT NOISE BASED DYNAMIC ACOUSTO-ELASTIC TESTING

Having access to the external strain by means of tidal models and to the velocity changes measured with ambient seismic noise we can reproduce in-situ a laboratory experiment for the investigation of elastic nonlinearity called dynamic acousto-elastic testing (DAET)[8, 9]. In

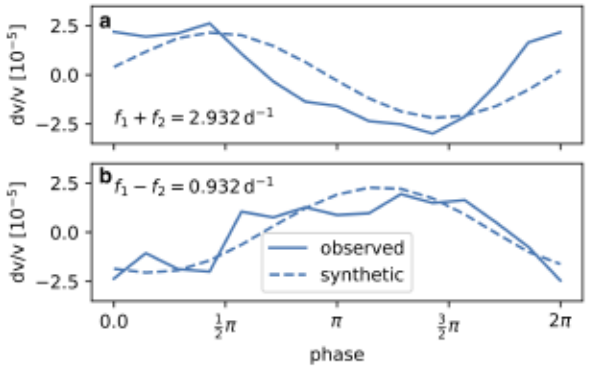

FIG. S2. Nonlinear interaction of the M_2 and S_1 signals. **a**) observed and synthetic signals for the modulation signal at 2.932 d^{-1}, **b**) same for the signal at 0.932 d^{-1}. Synthetic signals are calculated for a constant $C = -1000$ and match the observation at the sum and the difference of the S_1 and M_2 frequencies both in amplitude and phase.

DAET one observes the changing velocity of a small amplitude acoustic or elastic probe wave during the dynamic excitation of the target medium with a pump wave of large amplitude. In-situ field measurements have been performed using a vibrator truck to generate the pump wave[10]. We use the perturbation excited by moon and sun as pump wave and the ambient seismic noise waves to probe the velocity.

In Figure S3 we show the velocity variation as a function of volumetric strain for the M_2 tide. This means cyclic averaging with the frequency of the M_2 tide (1.932 d^{-1}) is applied to the strain and velocity signals of the 11 years observation as in Figure S1b. To isolate the effect of temperature, we split the data into four groups according to the phase ϕ in the diurnal temperature cycle (low, increasing, high and decreasing temperatures). As in figures S1 and S2 the phase is measured with re-

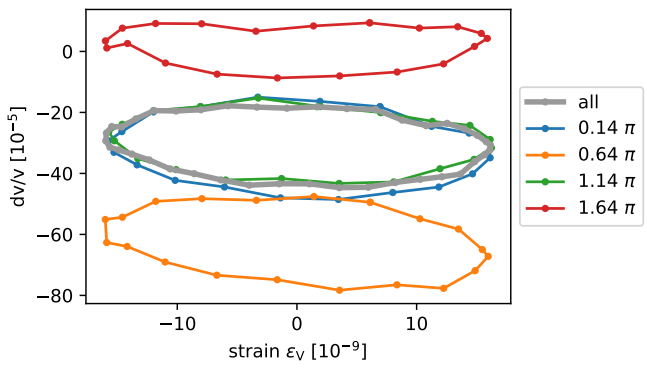

FIG. S3. Dynamic acousto-elastic testing with the M_2 tidal strain signal and noise correlation monitoring with a single seismic station. Strain and velocity values are obtained by cyclic averaging both signals with the period of the M_2 tidal constituent. Data is sub-grouped according to the phase of the S_1 cycle (time of the day) to separate the effect of solar radiation.

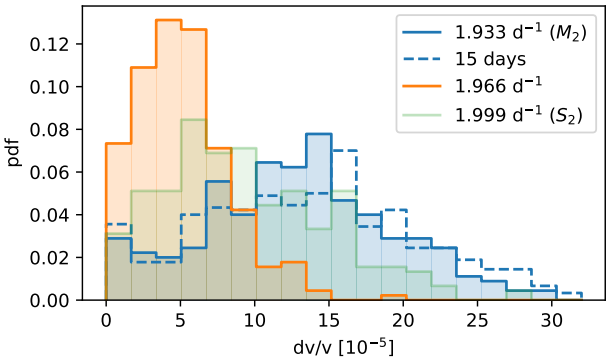

FIG. S4. Probability densities of the spectral amplitudes at different periods obtained from short time series. Continuous lines indicate measurements from 30 d long time series at the spectral peaks of M_2, S_2 and in between. The dashed line indicates probability density of the M_2 signal obtained from 15 d long time series.

spect to the beginning of the observation at January 1 2007, 00:00 UTC. The velocity follows four rather simple elliptical loops that fluctuate around different mean values according to the phase in the temperature cycle. As expected from the 2.5 h phase shift between the two almost sinusoidal strain and velocity signals observed in Figure S1b the curves are almost circular (for an appropriate aspect). Comparison between the curves for $\phi = 0.64\pi$ and $\phi = 1.64\pi$ shows that the amplitude of the velocity variation is larger for $\phi = 0.64\pi$ corresponding to low temperatures than during high temperatures at $\phi = 1.64\pi$. Apparently the velocity response to strain perturbations changes depending on temperature, directly illustrating the nonlinear coupling between the tidal and thermal strain perturbations (supplement section V).

VII. OBSERVATIONS WITH SHORTER TIME SERIES

The requirement for a reliable estimate of the velocity-strain sensitivity is the separation of the tidal contribution from environmental effects. Splitting the 11 years of observation into 30 d and 15 d long segments we investigate the possibility to observe the tidal signal from shorter time series. A measurement duration of 15 d ensures the mapping of the S_2 and M_2 tidal constituents on adjacent samples of a discrete Fourier transform. With 30 d of observation a separate spectral amplitude can be measured between the S_2 and M_2 frequencies which allows to observe the trough between the two peaks.

Figure S4 shows histograms of the spectral amplitudes of the M_2 and S_2 signals obtained from 30 and 15 days long time series. For the 30 days observation Figure S4 illustrates the ability to separate observations at 1.966 d^{-1} (between M_2 and S_2) from the signal at the M_2 frequency. The histogram of the M_2 spectral amplitudes obtained from 15 d time series is shown with a dashed line indicating that dv/v can be estimated with a uncertainty of about 50 %.

VIII. DEPTH SENSITIVITY OF VELOCITY CHANGES

The high precision of our measurements is achieved by using scattered waves contained in the coda of the noise correlation functions. A consequence of using scattered waves with a mixtures of body and surface waves is an uncertainty in the spatial sensitivity of the measurements. Surface waves in the investigated frequency range would have 90 % of the sensitivity confined in the top 200 meter[11] with the top 100 meter dominating the observations. Since we observe decreasing amplitudes of velocity changes for measurements at larger lapse times we conclude that (A) there is a body wave contribution to the sensitivity[12] and (B) the velocity changes are restricted to the shallow subsurface sensed by the surface waves.

In addition to the concentration of measurement sensitivity at the surface we can assume that the elastic nonlinearity which is at the origin of the velocity variations decreases with depth due to an increase in confining pressure. Our observations are thus representative for the top 100 meters.

Since surface waves[13] as well as scattered body waves[14] are most sensitive to variations in the shear wave velocity our measurements represent changes in the shear wave velocity.

[1] L. Krischer, T. Megies, R. Barsch, M. Beyreuther, T. Lecocq, C. Caudron, and J. Wassermann, Comput. Sci. Discov. **8**, 1 (2015).

[2] C. Sens-Schönfelder and U. Wegler, Geophys. Res. Lett. **33**, 1 (2006).

[3] C. Hadziioannou, E. Larose, and O. Coutant, J. Acoust. Soc. Am. **125**, 3688 (2009).

[4] T. Richter, C. Sens-Schönfelder, R. Kind, and G. Asch, J. Geophys. Res. **119**, 4747 (2014).

[5] C. Sens-Schönfelder, E. Pomponi, and A. Peltier, J. Volcanol. Geotherm. Res. **276**, 32 (2014).

[6] C. Sens-Schönfelder, Geophys. J. Int. **174**, 966 (2008).

[7] F. Brenguier, M. Campillo, T. Takeda, Y. Aoki, N. M. Shapiro, X. Briand, K. Emoto, and H. Miyake, Science (80-.). **345**, 80 (2014).

[8] G. Renaud, J. Rivière, P. Y. Le Bas, and P. a. Johnson, Geophys. Res. Lett. **40**, 715 (2013).

[9] J. Rivière, G. Renaud, R. A. Guyer, and P. Johnson, J. Appl. Phys. **114**, 1 (2013).

[10] G. Renaud, J. Rivière, C. Larmat, J. Rutledge, R. Lee, R. Guyer, K. Stokoe, and P. Johnson, J. Geophys. Res. Solid Earth **119**, 6907 (2014).

[11] M. Gassenmeier, C. Sens-Schönfelder, T. Eulenfeld, M. Bartsch, P. Victor, F. Tilmann, and M. Korn, Geophys. J. Int. **204**, 1490 (2016).

[12] A. Obermann, T. Planes, E. Larose, C. Sens-Schönfelder, and M. Campillo, Geophys. J. Int. (2013), 10.1093/gji/ggt043.

[13] J. Xia, R. D. Miller, and C. B. Park, GEOPHYSICS **64**, 691 (1999).

[14] H. Sato, M. Fehler, and T. Maeda, *Seismic Wave Propagation and Scattering in the Heterogeneous Earth*, 2nd ed. (Springer, Heidelberg, 2012) p. 494.